February 2019
Master's Degree Thesis

Analysis of UWB band-notch antenna with characteristics slots and MIMO antenna with resonating structure

Graduate School of Chosun University

Department of Information and Communication Engineering

Jiwan Ghimire

Analysis of UWB band-notch antenna with characteristics slots and MIMO antenna with resonating structure

February 25, 2019

Graduate School of Chosun University

Department of Information and Communication Engineering

Jiwan Ghimire

Analysis of UWB band-notch antenna with characteristics slots and MIMO antenna with resonating structure

Advisor: Prof. Dong-You Choi

A thesis submitted in partial fulfillment of the requirements for a master's degree in engineering

October 2018

Graduate School of Chosun University

Department of Information and Communication Engineering

Jiwan Ghimire

This is to certify that the master's thesis of

Jiwan Ghimire

has been approved by examining committee for the thesis requirement for the master's degree in Engineering.

Committee Chairperson

Prof. Goang-Seog Choi _____

Committee Member

Prof. Goo-Rak Kwon _____

Committee Member

Prof. Dong-You Choi _____

November 2018

Graduate School of Chosun University

Table of contents

List of figures

List of tables

Abstract

Analysis of UWB band-notch antenna with characteristics slots and MIMO antenna with resonating structure

Jiwan Ghimire
Advisor: Prof. Dong-You Choi, Ph.D.
Department of Information and Communication Engineering
Graduate School of Chosun University

The demand of various service applications within the same antenna, such as a multi-notch frequency band for mitigating interference with other narrowband communication systems, to overcome multipath fading, improve channel capacity and ensure link quality, has inspired the development of miniaturized antennas that are compact and simple in design complexity. However, because of the many wide bands working under the ultra-wideband (UWB) system, collision of these narrow bands is inevitable. Similarly, decoupling and coupling elements are introduced to enhance the isolation in between the two antennas where size compactness and isolation minimization are the main challenges in the design of multiple-input, multiple-output (MIMO) antenna for UWB communication. The proposed work in this thesis is to present a new design approach of adding formulated slots for multiband

rejection to the UWB antenna without any increase in size or additional expenses. Similarly, high isolation UWB MIMO antenna is designed introducing the parasitic resonator below the radiating patch in MIMO antenna helps to improvise the Isolation of the antenna without using any coupling or decoupling structure.

In present work two different type of antenna has been discussed:

Firstly, the design of a compact ultra-wideband U-shaped slot etched on a circular patch antenna exhibiting notch band characteristics for UWB applications. Four U-shaped slot structures are introduced based on a theoretical formulation where the formulation is validated with the equivalent LC lumped parameters responsible for yielding the notched frequency. A novel feature of this approach is that the frequency notch can be adjusted to desired values by changing the radial length based on the value calculated using a derived formula for each semi-etched U-slot, which is very simple in structure and design. Additionally, by introducing the rectangular notch at the ground plane, the upper passband spectrum is suppressed while maintaining the wide impedance bandwidth of the antenna applicable for next-generation wireless communications, 5G. The measured result shows that the antenna has a wide impedance bandwidth of 149% from 2.9 to 20 GHz, apart from the four-notched frequencies at 3.49, 3.92, 4.57, and 5.23 GHz for a voltage standing wave ratio (VSWR) < 2 rejecting the Worldwide Interoperability for Microwave Access (WiMAX) band at (3.38□3.7 GHz), the European C-band at (3.84□4.29 GHz), the Indian national satellite (INSAT) at (4.47□4.92 GHz) and wireless local area networks

(WLANs) at (5.09-5.99 GHz). The LC equivalent notched frequency has been proposed by analyzing the L and C equivalent formula, and it has been validated with simulated and measured results. The measurement and simulated results correspond well at the LC equivalent notch band rejecting the existing narrowband systems.

Secondly, the design of compact high isolation UWB MIMO antenna with a circular parasitic element at back side of the radiating patch thereby creating the reverse coupling helping to reduce the mutual coupling at upper part of the frequency bands and a small rectangular notch at the ground plane to extend the impedance bandwidth of monopole antenna. This approach eliminates the use of complex coupling or decoupling structure and complex feeding network. A novel feature of this design is that the MIMO antenna exhibits a very low envelope correlation coefficient (ECC < 0.007) with high diversity gain (DG > 9.99) and wide impedance bandwidth of 139 % from 3.1 to 17.5 GHz applicable for not only UWB application but also for next generation wireless communication, 5G. The high peak gain over the entire UWB and the upper part of the overall frequency band ensure that the antenna can be used in MIMO applications owing to the close agreement between the simulated and measured results.

The antenna is designed using finite element method based High Frequency Structure Simulator (HFSS) and their performance is analyzed on the basis of the reflection coefficient, VSWR, radiation patterns, gain, efficiency, ECC and DG.

요 약

슬롯 특성을 갖는 UWB 대역 노치 안테나와 공진 구조를 갖는 MIMO 안테나 분석

Jiwan Ghimire
Advisor: Prof. Dong-You Choi, Ph.D.
Department of Information and Communication Engineering,
Graduate School of Chosun University

기존 협대역 통신 시스템 간의 간섭을 줄이기 위해 다중 노치(multi-notch) 대역을 갖는 안테나 외에 다양한 어플리케이션 환경에서 다중 경로 페이딩의 극복, 채널 용량의 향상 및 링크 품질을 보장하기 위한 안테나 설계가 요구되어지고 있다.

그러나, UWB 시스템의 넓은 대역폭으로 인하여 기존 협대역 통신 시스템과의 충돌은 불가피하다. 또한, UWB 통신에 사용되는 MIMO 안테나의 경우 소형화가 주요 과제이며, 다수의 안테나 간의 격리 특성을 향상시키기 위해 디커플링(decoupling) 및 커플링(coupling) 소자가 도입되었다. 본

논문에서 제안한 UWB 안테나는 다중 대역 노치 특성을 갖는 슬롯을 추가하여 구조적 증가 및 추가 비용 없이 새로운 설계 접근 방식을 제안하였다. UWB MIMO 안테나의 경우 복사 패치의 후면에 기생 공명기를 추가하여 디커플링 및 커플링 구조 없이 우수한 격리 특성을 갖도록 설계하였다.

본 논문에서는 두 가지 유형의 안테나를 설계하여 분석하였다.

첫 번째 UWB 대역 노치 안테나는 UWB 어플리케이션 시스템에서 동작하는 원형 패치 안테나에 노치 밴드 특성을 갖는 U 형 슬롯을 추가하여 설계하였다. 4 개의 U 형 슬롯 구조는 LC 등가회로와 이론에 기반하여 검증하였다. 제안한 U 형 슬롯은 구조적으로 단순하며, 유도된 공식을 기반으로 하여 방사형 길이를 조절함으로써 원하는 주파수 대역을 조정하였다. 또한, 접지면에 직사각형 노치를 삽입함으로써 차세대 무선 통신인 5G 에 적용할 수 있는 넓은 임피던스 대역폭을 유지하면서 상위 통과 대역 스펙트럼을 억제하였다. 측정 결과, 2.9~20 GHz 까지 전압정재파비(VSWR)<2 를 달성하여 149%의 넓은 임피던스 대역폭을 보이며, 3.49, 3.92, 4.57, 5.23 GHz 의 4 개 노치 주파수 대역을 통해 WiMAX (Worldwide Interoperability for Microwave Access)의 3.38~3.7 GHz 대역, 유럽의 C 대역인 3.84~4.29 GHz 대역, 인도 국가 위성의 4.47~4.92 GHz 대역, WLAN (Wireless Local Area Networks)의 5.09~5.99 GHz 대역을 억제할 수 있었다. LC 등가 회로 노치 주파수는 L 및 C 의 등가 공식을 통해 제안하였으며, 시뮬레이션 및 실제 측정 결과와 비교하여 검증하였다.

시뮬레이션 및 측정 결과, 노치 대역이 기존의 협대역 시스템의 대역과 일치함을 확인할 수 있었다.

두 번째 MIMO 안테나는 복사 패치 후면에 기생 공명기를 갖는 UWB 용 MIMO 안테나로서 고주파수 대역에서의 상호결합과 직각 노치로 확장되는 역방향 결합이 가능하다. 이러한 접근 방식은 기존의 디커플링 및 커플링 구조와 복잡한 공급 구조를 사용하지 않아도 된다. 제안한 안테나는 DG>9.99 의 높은 다이버시티 이득을 가지며, ECC<0.007 의 매우 낮은 포락성 상관 계수를 보인다. 제안한 주파수 대역 내에 시뮬레이션 및 실제 측정 결과에서 높은 이득이 관찰되어 MIMO 어플리케이션에 요구되는 성능에 일치됨을 확인할 수 있었다.

제안한 두 안테나는 HFSS (High Frequency Structure Simulation) 툴을 사용하여 설계되었으며, 반사계수, VSWR, 방사패턴, 이득, 효율, ECC 및 DG 등을 통해 성능을 분석하였다.

1. Introduction

1.1 Overview

Modern wireless communication systems use the UWB system because of its advantages of smaller size, lesser complexity, and its provisioning for various service applications on different frequency bands with high-speed data rates and high time-domain resolution. Furthermore, multiband UWB microstrip patch antennas are popular for their simple features, including low profile, low manufacturing cost, simple feeding, and easy integration with active circuit components [1–3]. Moreover, the demand of various service applications within the same antenna, such as a multi-notch frequency band for mitigating interference with other narrowband communication systems, has inspired the development of miniaturized antennas that are compact and simple in design complexity. Because the antenna requires less power, it can be integrated with other portable internet of things (IoT) applications, surveillance systems, wireless body area networks (WBANs), and sensing and imagining applications that support all the data communication system bands [4–7]. However, because of the many wide bands working under the UWB system, collision of these narrow bands (e.g., the Worldwide Interoperability for Microwave Access (WiMAX) operating at 3.3□3.6 GHz, the European C-band at 3.8□4.2 GHz, the Indian national satellite (INSAT) at 4.50□4.80 GHz, and wireless local area networks (WLANs) at 5.15□5.825 GHz is inevitable. Solving this problem may give rise to complications of increased size and cost and insertion loss for the UWB system.

Band notch antenna techniques by etching thin slots in the radiating surface of an antenna or ground plane can be used for making multiband antennas and

producing a notch at lower frequencies by prohibiting interference between UWB and other narrowband systems without any increase in size or additional expenses. To suppress such potential interference, several design configurations have been proposed by modifying either the ground or the radiating patch or both by grooving various shapes (e.g., etching L-shaped, F-shaped, E-shaped, U-shaped, arc-shaped, or circular-shaped slots) to achieve the desired characteristics [8–16]. Adopting electrical and mechanical methods, as well as active filtering elements such as p-i-n diodes and varactor diodes, in different design methods enables reconfigurable antennas to be fabricated in terms of frequency band polarization and pattern and multipattern responses. However, the increased complexity, losses, and size of the system, coupled with the high power requirement, finally degrades the antenna electromagnetic (EM) characteristics [17]. Therefore, designing a UWB antenna using etching techniques for band-rejecting capabilities is the most suitable and economical solution to the problem. Triple-notch frequencies [18, 19], dual-notch frequencies [20–22], and single-notch frequencies [23–25] have been proposed using various design configurations either by adding tuning stubs or by etching slots. The addition of etching slots changes the current distribution and characteristic impedance along the radiating surface, contributing to perturbations in radiating modes by subsequently reducing the size of the antenna for realizing the given resonant frequency with a decreased quality factor (Q) value and proportionally increasing the bandwidth or establishing dual-band functionality [26]. However, placing the slots irregularly with a complex configuration in a radiating patch or a ground plane complicates the job of localizing the slots in the design and adds iteration time to the simulation design, making the process tedious. In addition, developing efficient

bandwidth enhancement with the band-notching technique in an area of limited size is still a difficult task.

The need for high data rates with efficient spectrum management utilizing multiple antennas in a single physical substrate is a recent requirement in modern wireless communication and UWB systems. For that MIMO technology takes advantage of multipath fading problems through diversity gain to improve link reliability, increase data throughput, and improve wireless capacity and range, which is not possible in a single-antenna system [27]. Even though MIMO technology is better than single-input, multiple-output (SIMO) or multiple-input, single-output (MISO) in terms of channel capacity, it has some limitations regarding the correlation between the antennas and realizing space efficiency [28]. Improving the isolation factor or correlation in a MIMO antenna using various types of coupling and decoupling structures is achieved at the expense of size and space.

Using decoupling structures such as active devices and passive resonators, defective ground structures (DGSs), electromagnetic bandgap, parasitic elements, neutralization lines, shortening pins, and loading slots on the antenna geometry to avoiding mutual coupling are proposed in various studies. In [29], a UWB amplifier was inserted to achieve wideband antenna matching and radiation efficiency; similarly, a passive microstrip-based feed network was introduced in [30] and a cylindrical dielectric resonator antenna (CDRA) in [31] for good MIMO operations at higher frequencies. The number of radiating element MIMO antenna systems were designed to improve isolation with DGS using different shapes (T, F, 4, arch) and slot lines; rectangular rings and ground slits were employed [32–38]. In [39], the electromagnetic bandgap structures were applied to closely placed arrays in the ground plane, resulting

in significant reduction of mutual coupling across the wide operating band. The use of parasitic monopoles helped to induce reverse coupling and hence to reduce mutual coupling in [40]. In [41], adding a neutralization line increased the effectiveness of the antenna system in term of isolation and bandwidth within a small space and without modifying the ground plane.

This thesis work describes a simple method to design a frequency-notched UWB antenna by adding a semicircular slot etched on the radiating patch surface. The notched frequency is tuned by changing the radius of the semicircular slot and the vertical etched slot whose length is half of the corresponding semicircular etched slot's radius. This arrangement is used to filter the unwanted frequency and avoid potential interference from narrowband communication systems within the UWB. In this work, we present the UWB effect by introducing slots on the antenna and compare the formulated notched frequency with the equivalent LC lumped model notch frequency. The antenna with a size of 25 mm × 25 mm × 1.62 mm is designed on a Taconic substrate and connected to a 50 Ω feedline. The feedline and patch are separated from the ground plane by the same length.

Similarly, the UWB MIMO antenna with enhanced isolation is proposed which has a very low mutual coupling ($|S_{21}/S_{12}| < -21$ dB). The presented MIMO antenna is composed of two monopole antennas with a common radiating surface. The two radiating patches are joined by two quad-circular structures. The ground plane is on the opposite side of the radiating patch and is etched so as to increase the impedance bandwidth characteristics. A circular parasitic element introduced at the center of the substrate acts as an isolator and exhibits low mutual coupling for the upper-frequency bands of the antenna. Without the presence of coupling or decoupling structures, good isolation is

obtained without the expense of increased size or adding complex structures. The results obtained from the designed UWB MIMO antenna reveal that it has good performance in terms of high impedance bandwidth and antenna gain, high radiation efficiency, high diversity gain, and low envelope correlation coefficient. The directional radiation pattern of the purposed MIMO antenna element proves that the antenna possesses good pattern diversity for a MIMO system.

1.2 Objectives

Interference in between UWB antennas and other narrowband communication systems has spurred growth in designing UWB antennas with notch characteristics and complicated designs consisting of irregular etched slots and larger physical size and also the need of high data rate with efficient spectrum management utilizing the multiple antennas in a single physical substrate (MIMO) is the recent requirement in modern wireless communication and UWB systems. The main goals and ideas of this research work are:

- To presents, a simplified notched design method for existing UWB antennas exhibiting four frequency-band-rejecting characteristics, validating the notched frequency with the equivalent LC lumped parameters.

- Implementing the parasitic elements to eliminates the use of complex coupling or decoupling structure and complex feeding network in UWB MIMO antenna.

1.3 Contributions

In this thesis, two UWB antenna design has been discussed. First one is a simplified notched design method for existing UWB antennas exhibiting four frequency-band-rejecting characteristics. The investigation has been conducted by introducing four semicircular U-shaped slot structures based on a theoretical formulation. The formulation is validated with the equivalent LC lumped parameters responsible for yielding the notched frequency. A novel feature of our approach is that the frequency notch can be adjusted to desired values by changing the radial length based on the value calculated using a

derived formula for each semi-etched U-slot, which is very simple in structure and design.

Similarly, the second one is the design of a compact high-isolation UWB MIMO antenna with a circular parasitic element at back side of the radiating patch, thereby creating the reverse coupling helping to reduce the mutual coupling at upper part of the frequency bands; and a small rectangular notch at the ground plane to extend the impedance bandwidth of the monopole antenna. This approach eliminates the use of complex coupling or decoupling structures and complex feeding networks. A novel features of our design is that the MIMO antenna exhibits very low envelop correlation coefficient (ECC < 0.007) with high diversity gain (DG > 9.99).

1.4 Thesis layout

Rest of this thesis is organized as follows. Chapter 2 provides the theory and background overview of the UWB and MIMO antenna. Chapter 3 discusses the detail design of UWB microstrip patch antenna and MIMO antenna. Under this section, a complete analysis is being made on simulated and measurement results where the antenna parameter are described on the basis of the reflection coefficient, VSWR, radiation pattern, gain, multiplexing efficiency and ECC with Diversity gain and Total active reflection coefficient (TARC). Similarly, a comparison is made with the existing antennas to validate its novelty. Finally, chapter 4 concludes the thesis and presents some conclusion of this study.

2. Theory and background

2.1 UWB technology

Since the Federal Communications Commission (FCC) released the spectral emission mask from 3.1□10.6 GHz with transmission power no more than -41 dBm/MHz for commercial UWB applications in 2002, the radio system has been getting increasingly popular in the industrial and academic field. In general, the existing UWB applications tend to be generic and highly specific and the designed antenna must be compact and good impedance matching, flat group delay and good omnidirectional radiation patterns in the presence of one or more overlapping channels. A typical UWB system will generate a pulse of data at lower power are transmitted over a wide spectrum which is usually useful for short ranged, low power consumption devises making feasible to run at low operating costs and within limited resources.

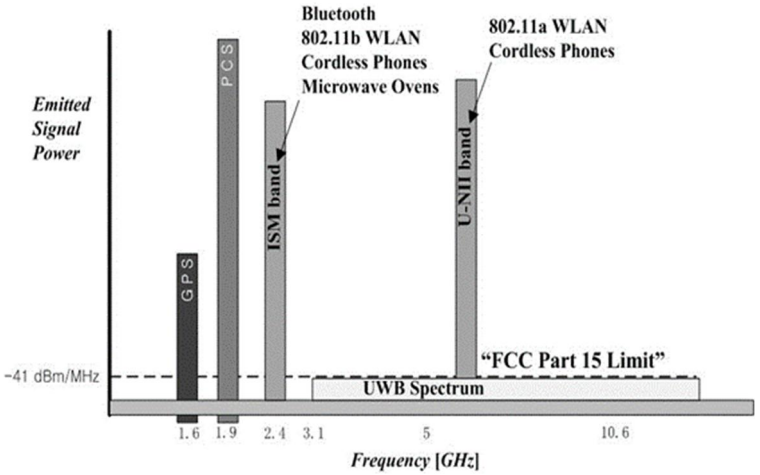

Figure 2-1. UWB versus other narrowband radio communication systems

Different technological applications involving within a scope of UWB including wall-imaging radar systems, medical applications, surveillance systems, vehicular radar systems, and wireless body area network (WBAN), Internet of Things (IoT), and communication and measurement systems. The signal spectrum of the UWB with other existing narrow-band systems is shown in Figure 2-1.

2.2 Characteristics of UWB

UWB is a new technology, which has substantial development potential in elementary areas like communication, automotive, localization services, security, imaging, and sensors. The growing number of media-intensive devices in the wireless personal area networks (WPANs) such as PCs, digital camcorders, digital cameras, high-definition TVs (HDTVs), gaming systems as well as the office devices such as cordless connection to peripherals, notebook, printer, PDA, fax machine, mouse, keyboard need a high bandwidth wireless solution for easy connection and media exchange. UWB radio is predicted as one of the most promising technologies for the above mention applications, due to its several advantages such as:

- **High bandwidth**: According to the FCC definition of UWB system, and transmitting system, which transmits signals in a bandwidth greater than 500 MHz or 20% bandwidth. UWB technology works in the bandwidth range of 3.1 GHz to 10.6 GHz
- **Low power spectral density**: The main reason for the UWB technology to coexist without causing interference to other services such as GPS, WLAN, WiMAX, Wi-Fi, and cellular network system is low power spectral density.

- **Low cost**: UWB technology did not require any carrier signal for transmission. Also, there is no need for a Radio Frequency (RF) converter or modulator. Hence, transmitters and receivers are simpler and easier to design and implement at a low cost.
- **Low power consumption**: UWB technology needs less than 1 mW of power to transmit hundreds of Kbps as far as 5 meters due to the absence of a carrier signal. Thus, UWB devices operate efficiently at low power levels.
- **High data transfer rates**: The data transmission is done over high transfer rates of 500Mb/s over 5m, 250Mb/s over 10m, 200Kb/s over 50m, 10Kb/s over 100m due to the availability of enormous amount of bandwidth.
- **Secure**: UWB technology operates on a wide bandwidth at a very low power level, which generates a low probability for intercept thus making it highly secure. Practically, it is highly difficult to filter a pulse signal from a background of electronic noise. Thus, it becomes almost impossible for an external user to detect the signal.

2.3 UWB MIMO antenna

Recently, there is a need of high data rate with efficient spectrum management in existing wireless communication systems. The application of diversity techniques with two or more than two antennas in a mobile terminal or in a single physical substrate can enhance the data rate , reliability and wireless capacity and ranges without sacrificing additional spectrum bandwidth or transmitted power in rich scattering and fading environments. MIMO UWB systems can further increase the channel capacity and range as compared to conventional SIMO or MISO systems for existing narrowband

applications within UWB. To combat the multipath fading problem in an indoor UWB wireless communication system, a UWB diversity antenna system is a promising candidate. However, for a MIMO antenna to be implemented in a multifunctional portable device, the following challenges are to be considered during the design of these antennas.

2.3.1 Design challenges in UWB MIMO antenna systems

- **Isolation**: Mutual coupling reduction between antennas is a major concern while designing MIMO systems. Mutual coupling not only affects the antenna efficiency but also influences the correlation, Diversity gain, multiplexing efficiency and total active reflection coefficient. Isolation better than -16 dB is required throughout the operating region of the antenna system.
- **Bandwidth:** Return loss (S_{11} in dB) should be less than -10 dB from 3.1 to 10.6 GHz and VSWR should be less than 2 so that the impedance bandwidth covers the entire UWB range. Synchronized enhancement of isolation factor and impedance bandwidth in a single antenna structure is one of the toughest challenges that exist in designing of a UWB MIMO antenna system.
- **Size:** MIMO has been adapted to mobile phones, which use various communication technologies such as WCDMA, WiMAX, WLAN, and UWB in order to realize high-speed data transmission, improve link reliability and wireless capacity and range and is not possible in the single-antenna system. To realise such an application requires a compact wide-band MIMO antenna system because of the limited space available in wireless devices.

Hence a compact UWB MIMO antenna system with low mutual coupling among the antennas is desired for UWB applications.

2.3.2 Isolation and bandwidth enhancement

Various coupling and decoupling methods and isolation structures techniques can be introduced for enhancement of bandwidth and isolation factor in a UWB MIMO antenna systems.

The mutual coupling can be reduced by introducing reflectors with a notch or adding complementary split-ring resonator (CSRR) on the ground plane. Adding stubs in some designs helps in reduction in mutual coupling. To increase impedance bandwidth, slots can be introduced in the patch. Several studies have been carried out on various MIMO antenna systems designs with two to four radiating elements. Various methods have been proposed to improve isolation between the antenna elements. Different structures like a mushroom, T, F,arch–shaped, EBG structures and slot lines have been proposed to reduce mutual coupling by suppressing the ground current flowing between the radiating elements. The low mutual coupling can also be achieved through neutralization techniques and decoupling networks, defected ground structures (DGS), adding rectangular rings. Ground slits are also introduced to improve antenna performance characteristics like size reduction, gain, and bandwidth enhancement, and they are also used in the reduction of mutual coupling between antenna elements.

3. Modeling of proposed antenna, simulations and measurement

3.1 U-shaped slot etched on a circular patch antenna with notch band characteristic

3.1.1 Design specification

The dimensions and geometry of the designed antenna is shown in Figure 3-1. The antenna consists of a monopole circular patch with radius R = 10.3 mm and feedline length F_L = 5 mm printed on a Taconic substrate with relative permittivity (ε_r) of 4.5 with a loss tangent of 0.0035. The ground plane serves as the impedance-matching circuit, whose impedance depends upon its width. A small rectangular notch is etched on the ground plane below the feedline to create a capacitive load that nullifies the inductive nature of the patch antenna and produces nearly resistive input impedance, especially at a higher band. Here, the return loss at the −10 dB lower frequency bandwidth is adjusted to $\lambda/4$ of the total combined length of the circular patch and feedline. Four semi-circular slots, of optimized radii of R_1 = 4.12 mm, R_2 = 4.705 mm, R_3 = 5.484 mm, and R_4 = 6.2 mm, are etched along with the vertical slot, each having a length half of the consecutive semi-circular slot radius. The formulated notch frequency for the related dimension is calculated in the following section as

$$f_n = \frac{c}{2L_n\sqrt{\frac{\varepsilon_r + 1}{2}}}, \quad (1)$$

where f_n is the notch frequency, c is the speed of light, and ε_r is the relative permittivity of the antenna substrate. The effective lengths L_n for notches n from 1 to 4 are calculated as

$$L_n = \pi\left(R_n + {}^{G}/_{2}\right) + 2S_n - G, \qquad (2)$$

where S_n is the slot's vertical length, which is half of the value of the radius R_n, and G is the width of the etched slot. Because of fringing, the total radius is the sum of the physical length of the radius R_n and the mean slot width. Similarly, because of fringing at the end of the vertical stub, its length gets reduced by the mean slot width.

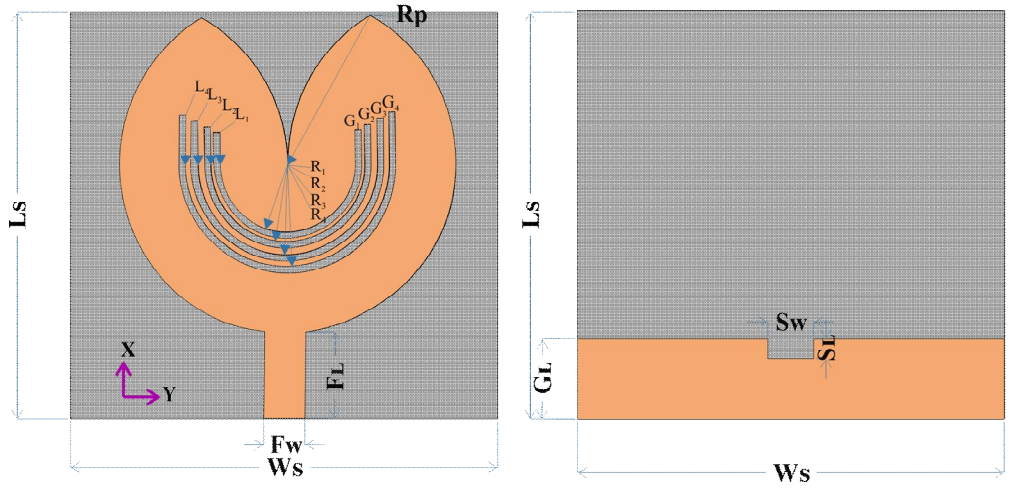

(a) (b)

Figure 3-1. Geometry of the antenna. (a)Top view, (b) Bottom view

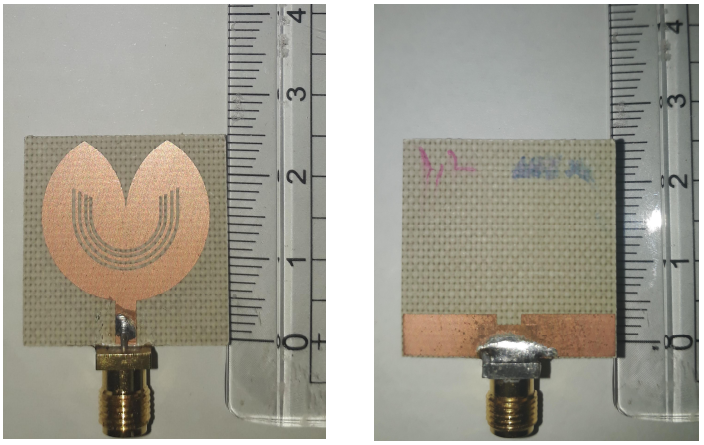

Figure 3-2. Antenna prototype top and bottom view

Table 1. Optimal dimension of the proposed UWB antenna

Parameter	Value (mm)	Parameter	Value (mm)
L_S	25	R_1	4.12
W_S	25	R_2	4.705
H_S	1.62	R_3	5.484
G_L	5	R_4	6.2
F_L	5.38	L_1	2.06
F_W	2.5	L_2	2.35
Rp	10	L_3	2.74
G_1, G_2, G_3, G_4, G	0.38	L_4	3.1
S_L	1.2	S_W	2.8

The optimized notching radii are selected based on a graph plotted between frequency and radii using Equations (1)□(2) as formulated notched frequency and Equations (3)□(7) as LC equivalent notch frequency. Figure 3-3 gives the graphical relation between the formulated notch frequency and the LC

equivalent notch frequency and shows that the formulated and LC equivalent notch frequency are almost close to each other for every semi-circular etched radius. The radius from the graph as determined with respect to each desired notch frequency is then used in the simulation and antenna fabrication and the results from the simulated notched frequency are compared to the measured results in Table 2.

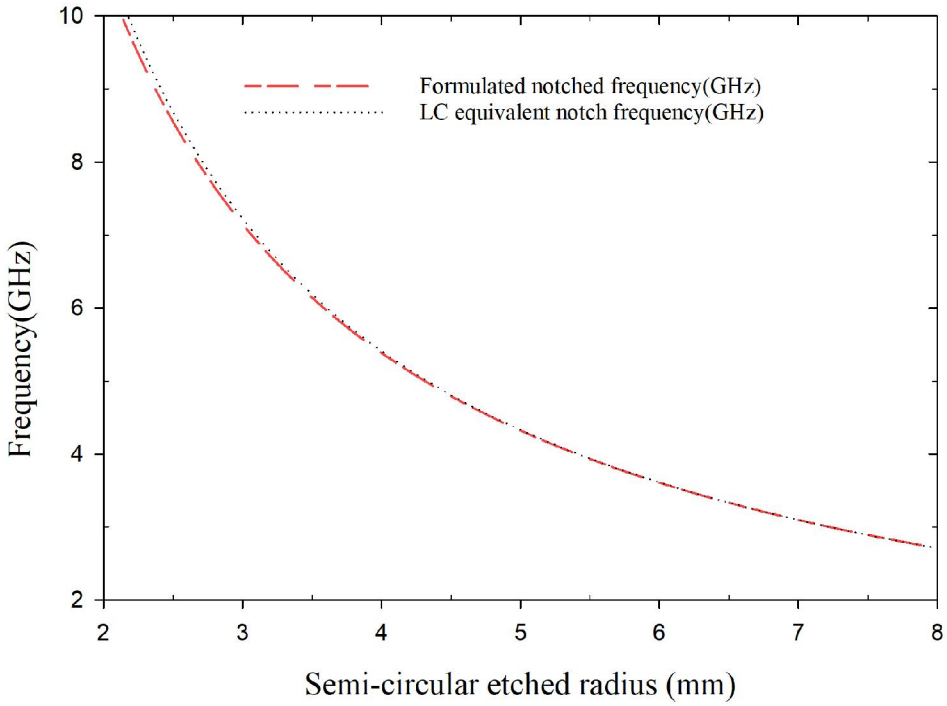

Figure 3-3. Graph of a formulated Vs. LC equivalent based on equations (1) and (3)

The LC equivalent notch resonant frequency f_0 of the etched slot is given by

$$f_0 = \frac{1}{2\pi}\sqrt{\frac{1}{L_{eq}C_{eq}}}, \tag{3}$$

where C_{eq} is the total equivalent capacitance of the slot structure, which is the sum of the combination of capacitances of the semicircular slot and the two vertical etched slots, along with the surface capacitance resulting from the charge on the surface of the etched slot. C_{eq} can be evaluated from [42]

$$C_{eq} = \varepsilon_0\left[\frac{\pi R_n t_P}{G} + \frac{2\pi t_P}{\ln\left(\frac{2\times 4t_P}{\pi R_n}\right)}\right] + 2\varepsilon_0\left[\frac{S_n t_P}{G} + \frac{2\pi t_P}{\ln\left(\frac{2\times 4t_P}{2S_n}\right)}\right] + \frac{2\varepsilon_o t_p}{\pi}\left[\ln\left(\frac{4R_s}{G}\right)\right], \tag{4}$$

where t_P is the thickness of the patch (generally 0.35 μm for a Taconic substrate) and G is the etched slot in the metallic patch, which is set the same for every etched slot. The slot length S_n is the vertical length, which is half the semicircular radius as mentioned earlier. The first section of the right side of Equation (4) is the parallel-plate capacitance resulting from air in the gap, the second part is a correction owing to fringing of the electric field at the etched slot edges, and the last section is the total surface capacitance resulting from the patch thickness and is calculated by assuming $R_s = G/2$. The equivalent inductance L_{eq} for the notched surface can be calculated by assuming the notch area as a wire of rectangular cross section having finite equivalent length l and thickness c in length equal to half of the slot's radius as proposed in as [43]

$$L_{eq} = 0.0002l\left(2.303\log_{10}\left(\frac{4l}{d}\right) - \theta\right)\ \mu H\,, \tag{5}$$

where the constant $\theta = 2.451$ is for a slot structure of circular geometry and depends upon the shape of the loop structure. Because the maximum etched portion has a semicircular geometry, the constant for the vertical slot that has a wire loop of the square is supposed to be equal to that of a semicircle and is included inside of the semicircular geometry for calculation. The effective equivalent length l and d can be evaluated as

$$l = 2L_n + G\,, \tag{6}$$

and

$$d = \frac{R_n}{2}\,. \tag{7}$$

The effective lengths L_n for notches n, is derived from Equation (2). Both the above equations are based on the analysis of the resonant frequency of a split ring and a simplified loop formula for regular figures. The parameters of the equations are based on the configuration of an etched slot structure. Because of the perturbation of the current distribution on the radiating patch by etching, the current has to take a longer path. This path determines the series inductance, whereas the thin gap of the etch is responsible for the accumulation of charge and consequently formation of the series capacitance [44]. This combined effect can be shown by the equivalent LC parameter lumped element circuit, which is expressed in Equations (4) and (5). The equivalent lumped element parallel RLC circuit model of the fabricated antenna is shown in Figure 3-4. L_i, C_i, R_i for (i = 1 to 4) are the inductance, capacitance and radiation resistance for i^{th} radiating mode at each resonant frequency band respectively. Each etched slot has a lumped effect that attenuates the frequency band and can be

represented as a series combination of every four lumped elements with a notched ground plane as a capacitive load and an inductive radiating patch. Capacitive (C) and inductive (L) effects are taken into account for higher order modes as well as feeding effect and are the dominant term for the input impedance of the antenna. In Figure 3-5, we see the equivalent input impedance (Z_{in}) of the antenna; the resistance varies around 50 Ω while its input reactance oscillates around zero. The maximum equivalent resistance is found in the notch bands while the equivalent reactance almost tends to zero. This is due to the RLC resonating condition, where capacitive impedance is equal to inductive impedance, which gets cancelled out, as the resistance part takes on that role. Impedance mismatch between the feedline and the radiating patch is responsible for the band-rejecting characteristics.

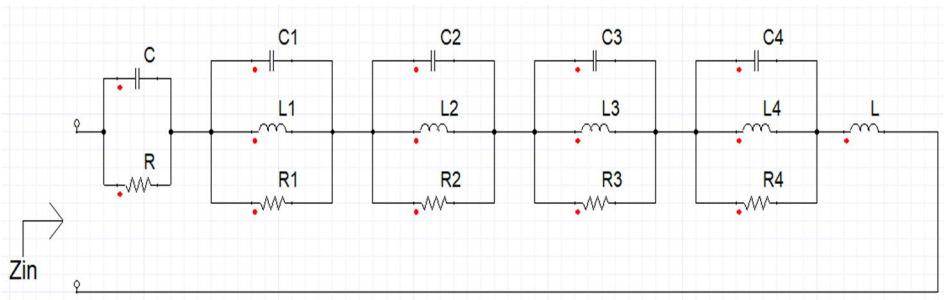

Figure 3-4. Equivalent lumped element circuit model

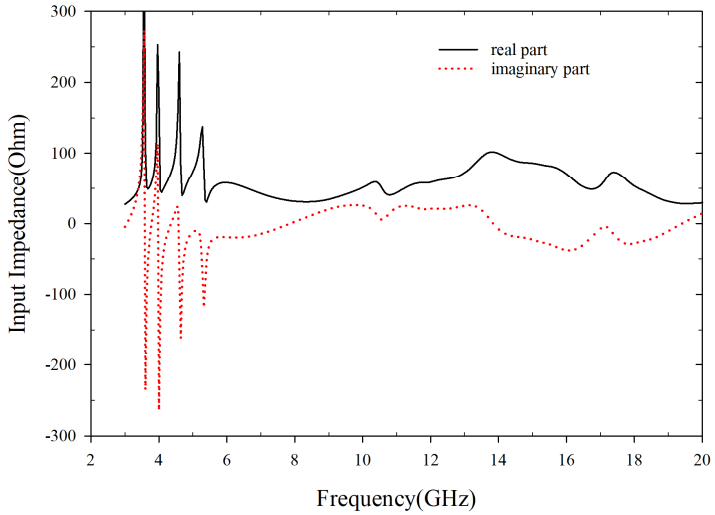

Figure 3-5. Input impedance of the proposed antenna

3.1.2 Design strategy

By using the layout of the prototype antenna shown in Figure 3-1, the individual effect of each etched slot of radial length R_n in a radiating patch on the VSWR is shown in Figure 6(a). The experiments are made on a Taconic substrate of relative permittivity (ε_r) = 4.5 with etched slots of 0.38 mm in width. By tuning the parameters R_1, R_2, R_3, and R_4, one can get the first, second, third, and fourth resonating frequencies for WIMAX, the European C-band, INSAT, and WLANs easily. Because the resonating frequency completely depends on the semicircular etched slot's radial length, we can shift the notching frequency to any desired ones. Figure 3 shows the graph where the plot gives slot radial length and this is taken into account in the simulation for the required corresponding notch frequency. Figure 6 shows the VSWR plots of various etched slots of the differing radial parameter. The increase in the VSWR at the notched frequency stopband can ensure high quality UWB

communication links by filtering coexisting narrowband interference. The frequency notches for consecutive slots are relatively less affected by the neighboring slots in terms of coupling issues, as each resonator slot is physically far away from another, being at least beyond the fringing field of each slot. Results from Table 2 comparing the LC equivalent notch frequency with respect to the simulated notched frequency also demonstrate that successive slots are relatively less affected by neighboring slots.

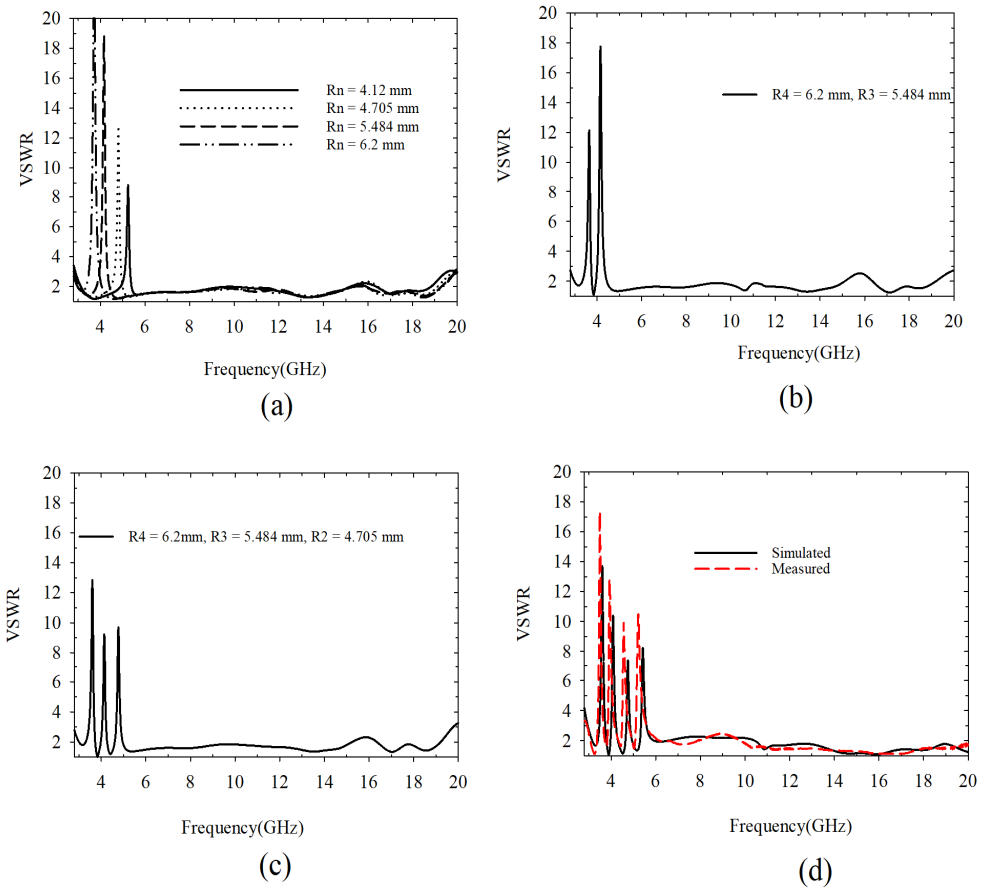

Figure 3-6. VSWR plot for different geometrical etched slot parameters.

Figure 3-6 presents a VSWR plot of the notch frequency for different geometrical etched slot parameters. Notch at the different frequency band from varying the parameter Rn can be seen in Figure 3-6 (a) whereas, Figure 3-6 (b) represent the notch at the WiMAX band and the C-band from parameters R4 and R3. Similarly, in Figure 3-6 (c), we see the notch at the WiMAX band, the European C-band, and INSAT band from parameters R4, R3, and R2. The Measured and simulated frequency notch at the WiMAX band, the European C-band, INSAT band, and WLAN band from parameters R4, R3, R2, and R1 is represented in Figure 3-6 (d) through VSWR plot.

Table 2 compares the formulated, simulated and measured notched frequency with the equivalent model of an LC lumped element circuit, represented by four parallel RLC resonators connected in series. At resonating conditions, the stopband frequency or cutoff frequency depends upon L and C, and it can be evaluated using Equations (4) and (5). The Lumped element equivalent resonance notched frequency computed using Equation (3) corresponds well with the measured and formulated values.

Table 2. Comparison table of LC equivalent lumped element

Notc-hes	R_n (mm)	Simu-lated notch-ed frequ-ency (GHz)	Meas-ured notch-ed freque-ncy (GHz)	Form-ulated theoret-ical frequ-ency (GHz)	Para-meter L (nH)	Para-meter C (pF)	LC equiva-lent notched freque-ncy (GHz)
1	4.12	5.32	5.23	5.23	67.278	0.0139	5.25
2	4.705	4.68	4.57	4.58	76.553	0.0158	4.6
3	5.484	4.03	3.93	3.94	88.904	0.0185	3.94
4	6.2	3.57	3.49	3.49	100.257	0.02	3.49

3.1.3 Measurement and simulation results

a. Antenna gain and radiation efficiency

The proposed antenna's final measured radiation patterns are shown in Figure 3-7. The measurements were taken in an anechoic chamber covering different passbands of the UWB. The radiation pattern in the x–z plane (E plane) is omnidirectional and it is nearly bidirectional in the y–z plane (H plane), which shows that the antenna radiates over a range of frequencies with minimum effect of band notching behavior on the antenna radiation patterns.

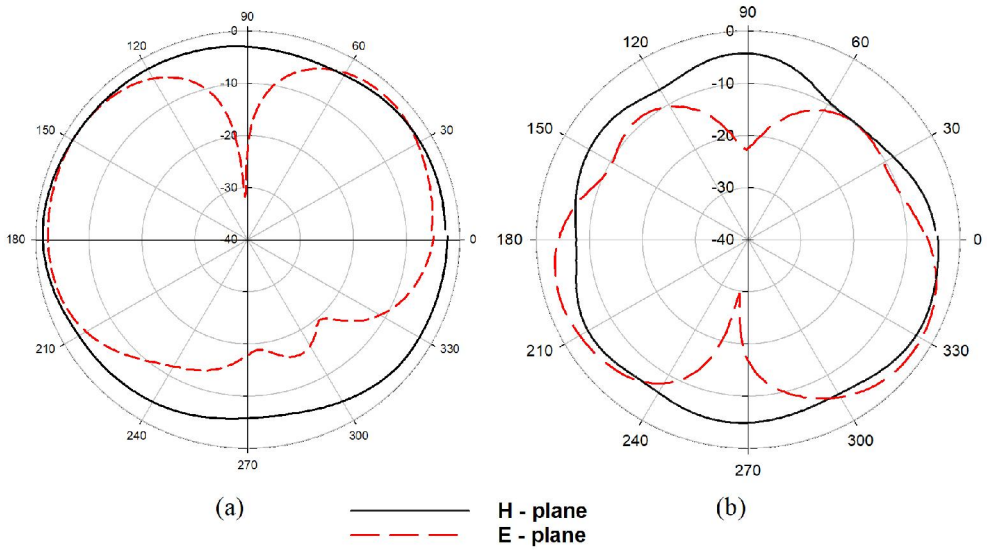

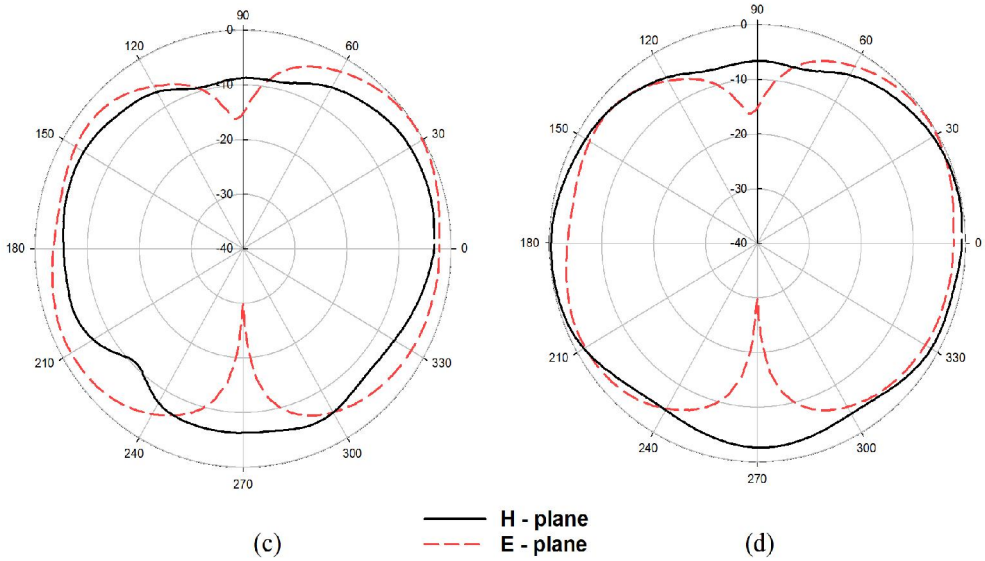

Figure 3-7. Measured radiation pattern at (a) 3.26, (b) 3.77, (c) 4.41, and (d) 5.02 GHz.

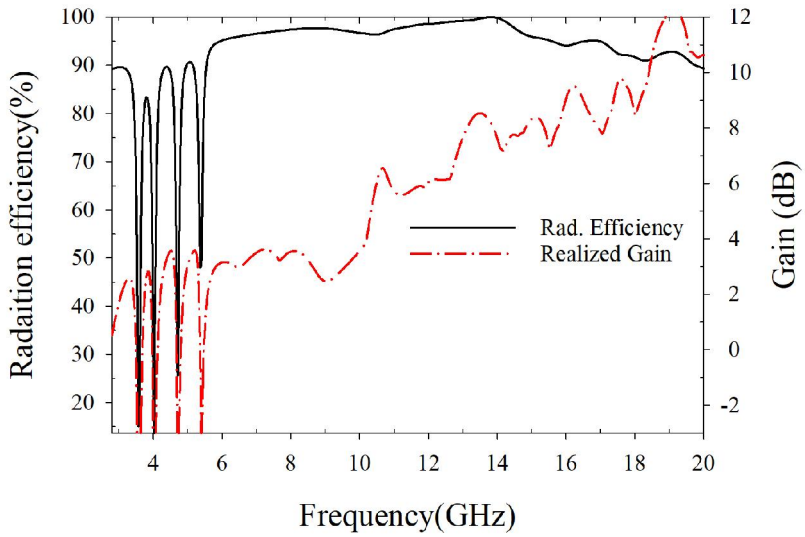

Figure 3-8. Simulated antenna gain and radiation efficiency

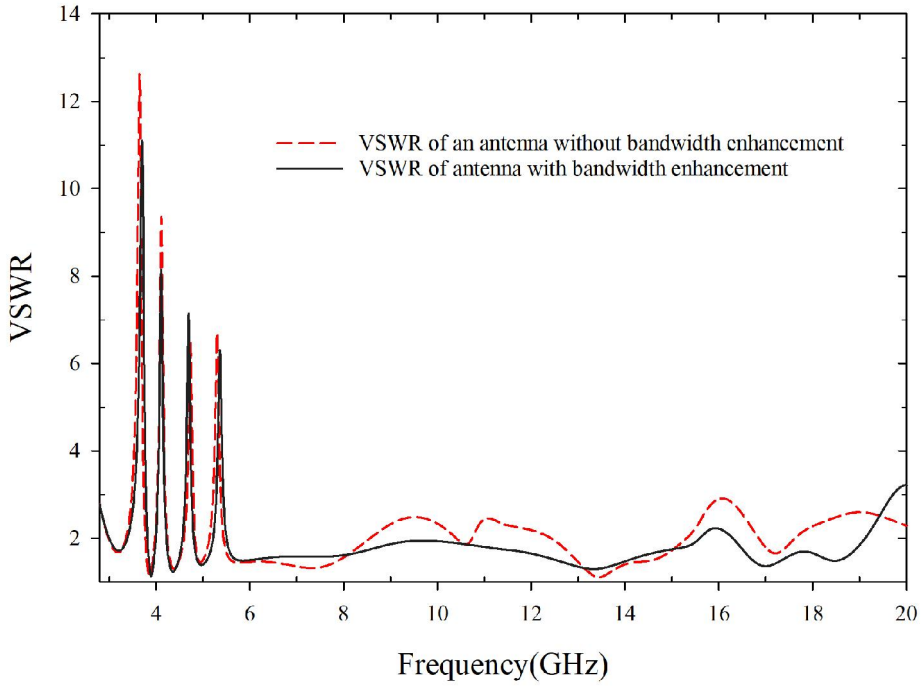

Figure 3-9. Simulated VSWR plot of the UWB antenna with ground notch versus without notch

In Figure 3-8, we can see that different etched slots on the antenna yield well-suppressed antenna gain and efficiency at the four places of the intended rejection band, indicating high interference at those frequencies. This clearly specifies the band-rejection characteristics of the semi-circular etched slot. Figure 3-9 depicts the change in impedance bandwidth by adding a rectangular notch of length SL and width Sw at the ground plane. By etching a small rectangular surface at the ground, beneath the feedline of the radiating patch, radical improvement in the bandwidth performance of the antenna was obtained which is suitable for working at immerging next-generation wireless communication, 5G. And also, when adding a notch at the ground plane, it is

seen that the effects on the notched frequency bands are negligible. Figure 3-10 shows the simulated surface current distribution at each rejection band at (a) 3.57 GHz. (b) 4.03 GHz. (d) 4.68 GHz. (e) 5.32 GHz. The surface current is seen to be concentrated mainly on the periphery of each semi-etched slot, which acts as a resonator, prohibiting signal propagation at that frequency.

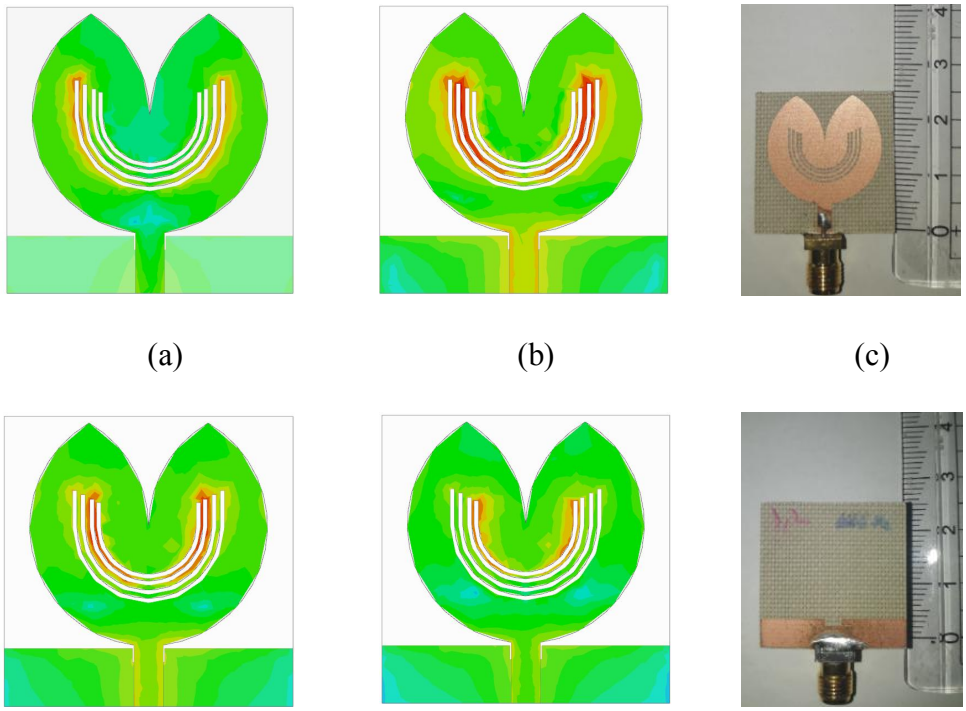

(a) (b) (c)

(d) (e) (f)

Figure 3-10. Simulated surface current distribution on the radiating patch of the antenna

b. Comparison with other references

To validate the performance of the antenna a comparison is made in Table 3 with other reported antennas owing the advantage of smaller size, a wider impedance bandwidth and complete rejecting bands with maximum VSWR parameter. As most of the antenna reported in the literature have irregularly placed parasitic stubs and resonators with asymmetrical itching on the radiating and ground surfaces as well as complexity in manufacturing design and structure, our proposed antenna has much advantage of placing regular symmetrical etched slot which is easy to tune, replicate and fabricate for the desired notch frequency bands.

Table 3. Comparison with other reported references

References	Size (mm)	Bandwidth (GHz)	Notched Bands (GHz)
[20]	20 × 27	2.89□11.52	3.4□3.69, 5.15□5.825
[21]	24 × 28	3.0□13.0	5.15□5.4, 5.725□5.94
[22]	38.5 × 46.4	2.0□12.5	5.0□5.5, 7.2□7.6
[23]	27 × 20	3.1□10.6	5.15□5.85
[24]	22 × 8.5	3.8□10.6	5.15□5.85
[25]	30 × 28	2.78□12.3	5.2□6.0
[45]	31 × 33	2.0□6.0	3.19□3.97, 4.92□5.86
[46]	66.3 × 66.3	3.1□10.6	3.6□3.9, 5.6□5.8
[47]	30.2 × 25	2.7□12.3	3.19□3.97, 5.16□5.85, 7.88□8.59
[48]	30 × 30	3.04□10.9	3.29□3.61, 4.65□5.49, 7.3□8.41
[49]	28 × 26	3.1□12.0	5.15□5.35, 5.75□5.85, 7.25□7.75, 8.01□8.55
[50]	40 × 40	2.1□11.0	2.37□2.9, 3.27□3.76, 5.2□5.89, 8.06□8.8
[51]	30 × 28	3.0□11.0	3.3□3.6, 4.5□4.8, 5.15□5.35, 5.7□5.825

Proposed work	25 × 25	2.9□20.0	3.38□3.7, 3.84□4.29, 4.47□4.92, 5.09□5.99

3.2 Bandwidth enhancement and mutual coupling reduction using notch and parasitic structure in UWB MIMO antenna

3.2.1 Design specification

The proposed geometry of the UWB MIMO antenna is shown in Figure 3-11. The antenna was designed on a Taconic substrate (ε_r = 4.5, tan δ = 0.0035). The size of the antenna is 65 mm × 65 mm × 1.62 mm. The antenna is composed of a microstrip patch with a common radiating patch and a ground plane designed on the top and bottom side of the substrate. Here, to meet the operating frequency requirement, the return loss at the −10 dB lower frequency bandwidth is adjusted to 3.1 GHz approximated using the following frequency.

$$f_n = \frac{c}{2l_t\sqrt{1+\frac{\varepsilon_r}{2}}}, \tag{8}$$

where, f_n is the first operating frequency, c is the speed of light in the vacuum and l_t is the combine total effective lengths of the circular patch radius R1 and R2. Moreover, a circular parasitic strip is placed at the ground plane along the center of the substrate to improve isolation between the monopole antennas. The feed line and a small notch in the ground plane, employed to obtain the line characteristic impedance of 50 Ω, are set to 1.8 mm and 4 mm × 5 mm, respectively. The radiating patch is structurally a combination of a quad circular structure with a semi-circle of half the radius of the quad circle placed at the top of it. The two radiating patches are commonly connected by two

small quad circular structures positioned opposite each other, where the circular parasitic strip is located below it. The need of connecting two radiating patch by a two small quad circle is to not only improve the isolation but also to have a common signal reference weather it is signal ground plane or the radiating patch. The split in the ground or patch is not practical since, in the real system signal should have the common reference plane so that all signal levels within the system can be interpreted properly based on that reference level [52]. However, the proposed design is similar to a microstrip patch antenna with feeding points placed opposite each other; the optimized antenna structure, with isolation enhancement without the use of coupling and decoupling structure, make it preferable in terms of bandwidth, diversity gain, and multiplexing efficiency, the significant parameters for any diversity antenna.

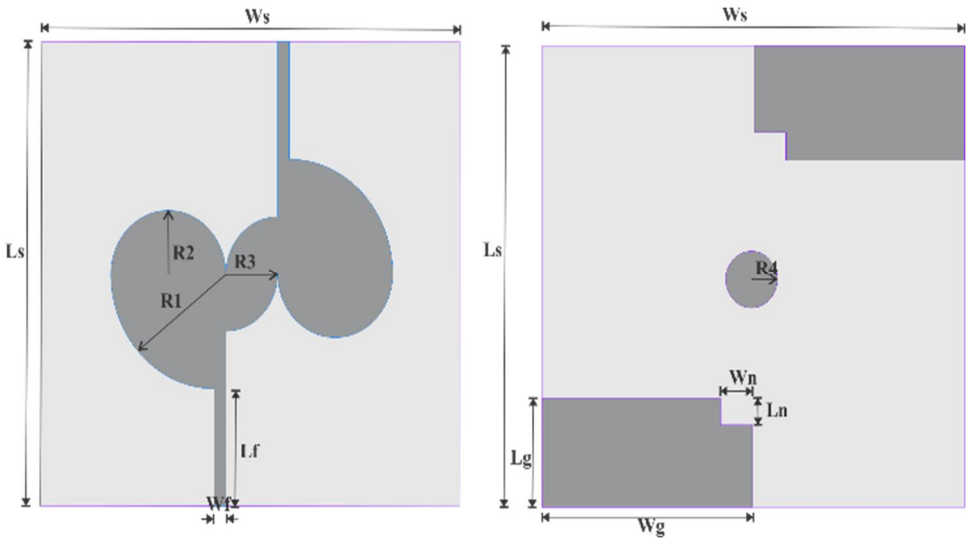

Figure 3-11. Geometry of the proposed UWB MIMO antenna

Table 4. Dimension of UWB MIMO antenna

Parameter	Dimension (mm)	Parameter	Dimension (mm)
Ls	65	Lg	16
Ws	65	Wg	32.7
Lf	16.3	Ln	4
R1	17.8	Wn	5
R2	8.9	Wf	1.8
R3	8	R4	4

3.2.2 Design strategy

Figure 3-12 illustrates the antenna design steps and the effect on the antenna bandwidth and mutual coupling. First, in Figure 3-12 (a), the antenna is designed with radiating patches facing indirectly opposite each other, which allows space utilization within a limited space of the antenna; and second, the geometrical structure of the radiating patch enables the MIMO antenna to be directional, which could supply good pattern diversity for the MIMO system. The simulated parameters of the antenna reflection coefficient (S_{11} and S_{21}) in Figure 3-13 (a) and Figure 3-13 (b) reviles that the antenna has poor isolation in higher frequency range and a high impedance mismatch in the entire UWB range for the antenna shown in Figure 3-12 (a). With the placement of two quad circular structure connecting two radiating patches (Figure 3-12 (b)), mutual coupling between the proposed antennas is reduced, but the characteristics line impedance of the antenna remain same as that of antenna design taken at first stage. Further, to improve the impedance bandwidth of the

antenna in whole UWB range a small rectangular etching is made at the ground plane (Figure 3-12 (c)). The etching not improves the characteristics line impedance but also decrease the isolation factors in the lower frequency spectrum of the proposed UWB MIMO antenna with a slight increase in isolation factor at upper-frequency range. A circular parasitic resonator is introduced at the backside of the substrate plane (Figure 3-12 (d)). The resonator is excited by the current flowing in the radiating patch. The excited reverse current on the resonator prevents the flow of current in the other radiating patch preventing it from further coupling and on appropriately designing the antenna configurations, the mutual coupling existing in between the radiating patch may be considerably reduced.

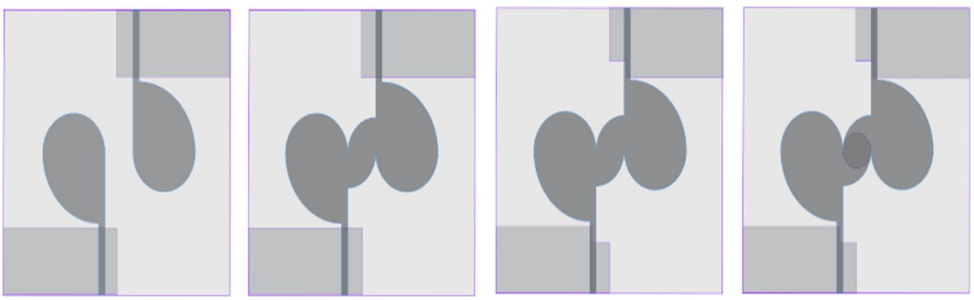

(a) (b) (c) (d)

Figure 3-12. Geometry of UWB MIMO antenna with different evolution steps

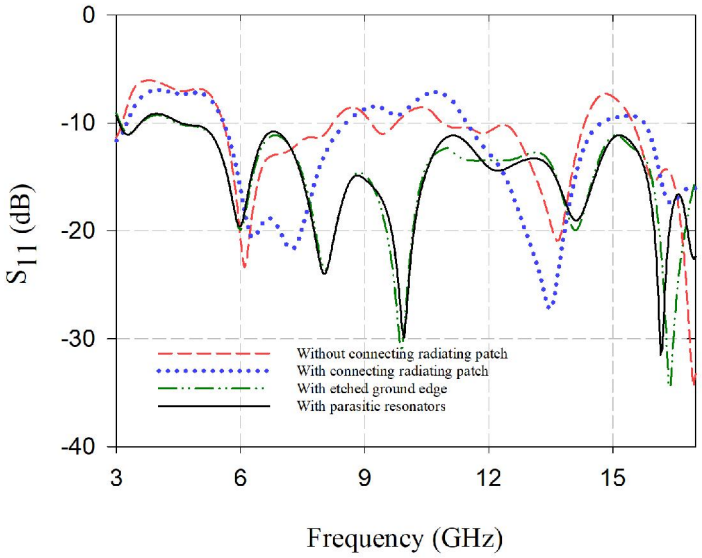

(a)

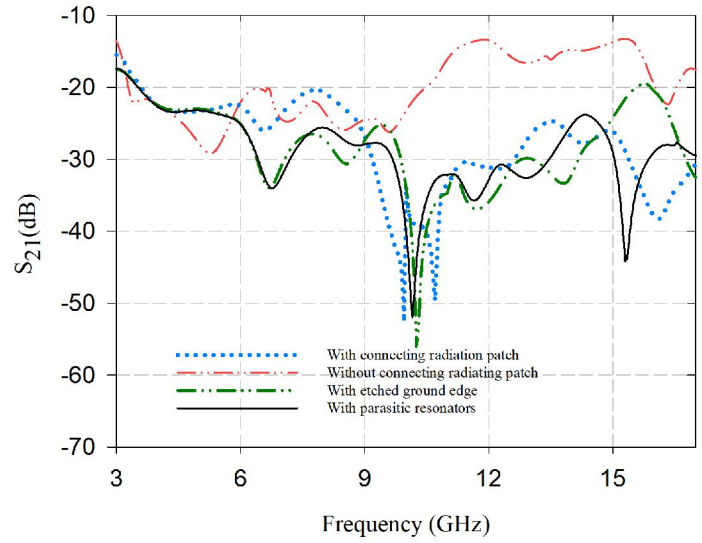

(b)

Figure 3-13. Simulated S-parameters illustrating on different stages of antenna variations

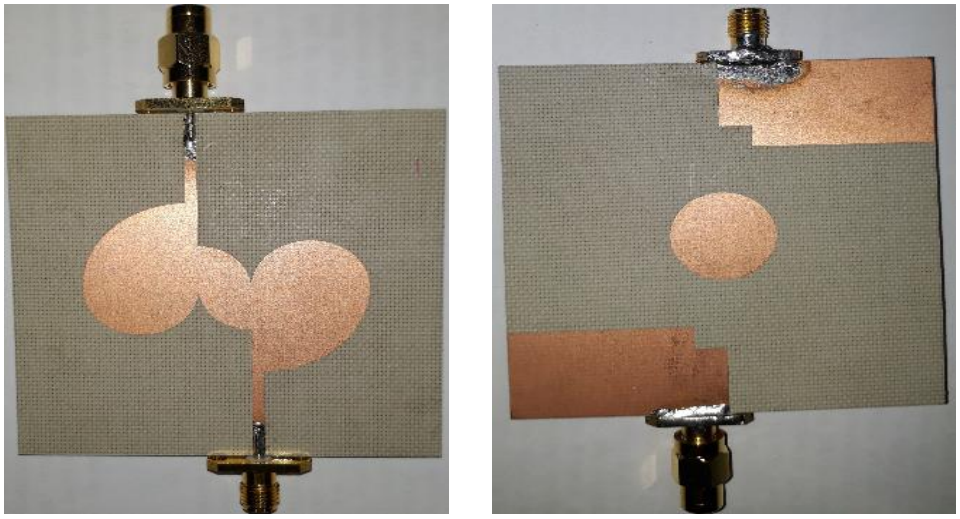

(a) (b)

Figure 3-14. Fabricated antenna design (a) top view and (b) bottom view

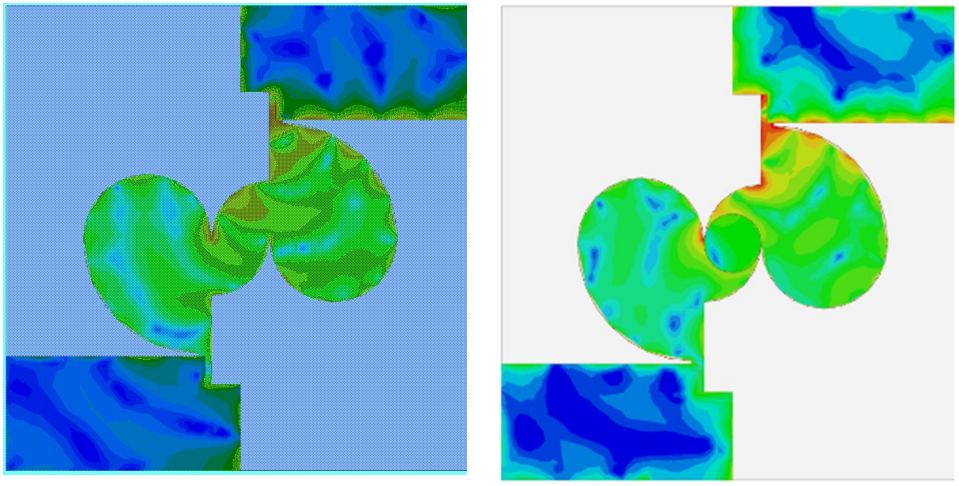

(a) (b)

Figure 3-15. Simulated surface current distribution at 16.5 GHz

The surface current distribution along the radiating and ground patch validates the performance of reducing the mutual coupling. As a comparison, the current distribution with and without the circular parasitic monopoles are plotted in Figure 3-15, when only one of the port is excited. On excitation, as shown in Figure 3-15 (a) high coupling is achieved at the other radiating patch and the ground plane because the current concentration is equally spread all around the patch and the plane significantly. By the insertion of the circular resonating structure depicted in Figure 3-15 (b), it can be observed that the current is concentrated at the radiating patch of the excited port and becomes trapped all around the periphery of the circular resonating structure. Because of this effect, the ground plane of the other radiator and the patch has coupled much less current concentration, and hence less isolation is achieved in between the two radiating patches. In addition, the simulation result shows that most of the current above 14.7 GHz is concentrated around the resonating patch, which explains the reducing mutual coupling (S_{21}) observed in Figure 3-13 (b).

3.2.3 Measurement and simulation results

The antenna is designed on a Taconic substrate having a relative permittivity of 4.5 with a thickness of 1.6 mm. For the optimization and simulation of the proposed antenna, a commercially available High frequency Structure Simulator (HFSS) software was used. The simulation and measurement result is shown in Figure 3-16; Figure 3-16 (a) shows impedance bandwidth with S_{11} < -10 dB from 3.1 to 17.5 GHz. The mutual coupling between the antenna in Figure 3-16 (b) is below -15 dB for 3.1□3.5 GHz and below -21 dB over 3.5 □17.5 GHz dB with close agreement between the measured and simulated

result. The simulated and measured reflection coefficient differs slightly and can be endorsed by the losses taking place in the connector, imperfect soldering and fabrication errors.

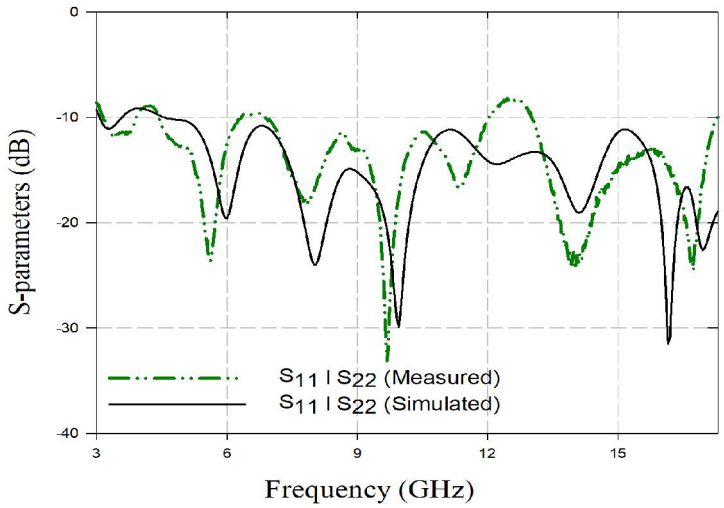

(a)

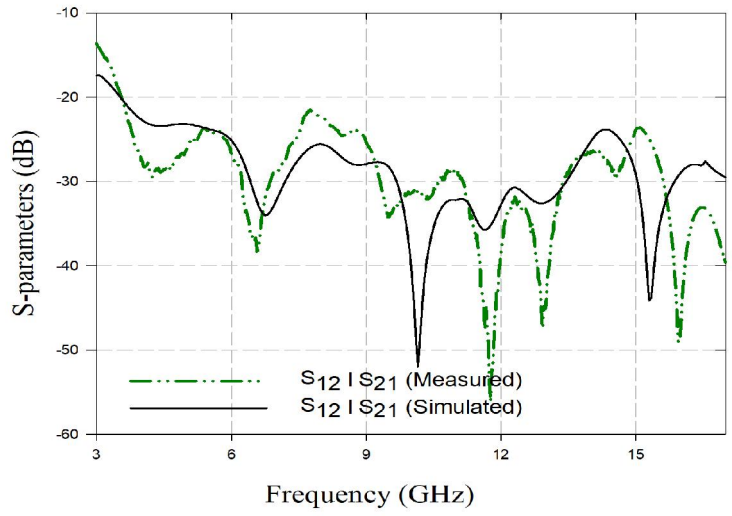

(b)

Figure 3-16. Simulated and measured results of S-parameter. (a) S_{11}/ S_{22} (b) S_{12}/S_{21}.

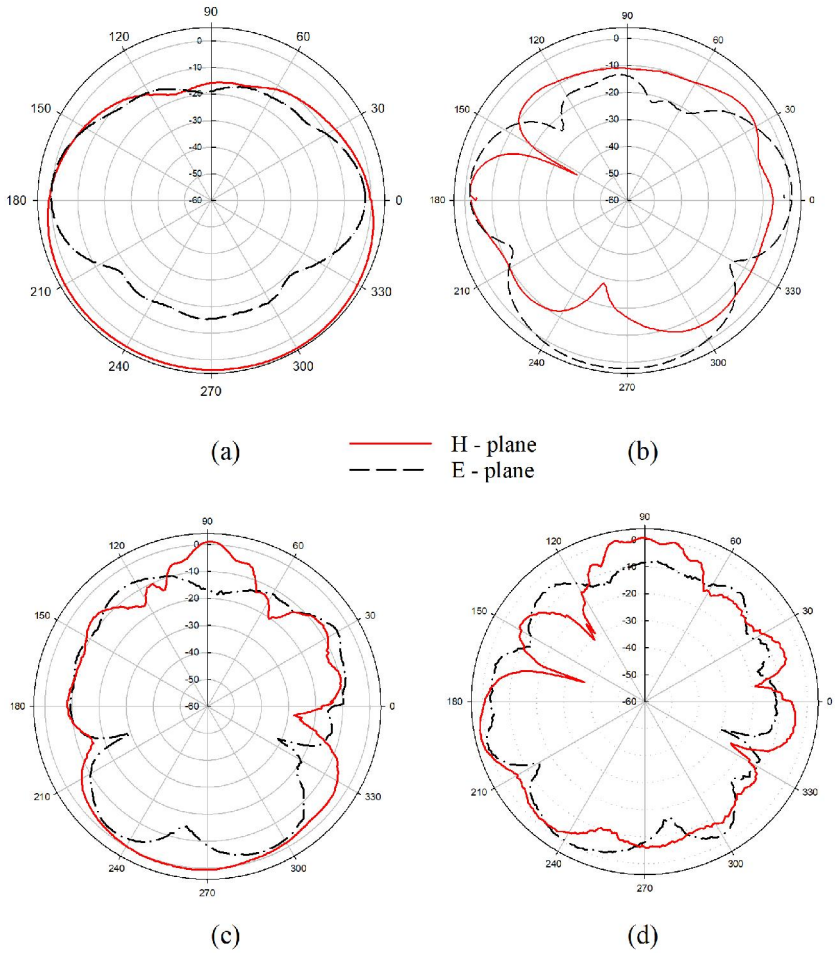

Figure 3-17. Measured radiation pattern at (a) 3.5, (b) 5.5, (c) 11.5, and (d) 16.5 GHz.

a. Antenna gain and radiation efficiency

The measured 2D radiation patterns are shown in Figure 3-17. The measurement was taken with one of the ports terminated by a 50 Ω load and vice versa. The radiation pattern is almost omnidirectional in both the E-plane

(x–z plane) and H-plane (y–z plane), which is one of the required characteristics for a MIMO antenna.

In order to verify the capability of the proposed MIMO antenna, ECC and DG between the antennas must be as low as possible; a lower ECC signifies higher pattern diversity. The ECC between the two radiating antenna elements can be calculated by [53] .

$$ECC = \frac{\left|S_{11}^{*}S_{12} + S_{21}^{*}S_{22}\right|^{2}}{\left(1-\left|S_{11}\right|^{2}-\left|S_{21}\right|^{2}\right)\left(1-\left|S_{22}\right|^{2}-\left|S_{12}\right|^{2}\right)}, \quad (9)$$

where, S_{11} and S_{22} are the antenna refection coefficient measured in two ports and S_{12} and S_{21} are the insertion losses of the antenna. Using the reflection coefficients and insertion losses of the antenna measured through the vector network analyzer (VNA), ECC is calculated and the result is plotted and shown in Figure 3-18. Conventionally, the overall effect of a MIMO antenna is characterized by diversity gain and MIMO capacity. However, MIMO capacity is the complicated function of the antenna parameters. To simplify the antenna design, a simple and intuitive metric like multiplexing efficiency and TARC are proposed. The multiplexing efficiency defines the losses or degradation of power efficiency required when using a MIMO antenna under test to achieve the same performance or capacity as that of a reference antenna system in the same propagation channel within uniform 3D angular power spectrum. The signal-to-noise ratio (SNR) degradation due to MIMO antenna –channel losses for a given MIMO capacity, η_{mux} is given by [54]

$$\eta_{mux} = \sqrt{(1 - |{\rho_c}^2|)\eta_1\eta_2}\,, \quad (10)$$

where $\eta_1\eta_2$ are the total efficiency of two radiating antenna elements and ρ_c represents the complex correlation coefficient between them. Since the total efficiency of the antenna is very high, for this ECC is nearly equal to $|\rho_c{}^2|$ .The DG of the proposed UWB MIMO antenna can be calculated using

$$DG = 10\sqrt{1 - ECC^2}\,. \tag{11}$$

Figure. 3-20 shows the plot of the TARC where the value of TARC of the proposed antenna is less than -1.3 dB for the entire frequency band. TARC calculate the actual antenna behavior by predicting the return loss of the overall MIMO antenna system and can be calculated by the following relations [55]

$$\mathrm{TARC} = \sqrt{\frac{(\mathrm{S}_{11} + \mathrm{S}_{12})^2 + (\mathrm{S}_{21} + \mathrm{S}_{22})^2}{2}}\,. \tag{12}$$

From Figure 3-18, all the ECC values are less than 0.007, and the DG is high, greater than 9.99 for the entire UWB band. The realized gain and the multiplexing efficiency are shown in Figure. 3-19 where its high measurement values on the entire frequency range make the antenna applicable for UWB, and 5G communication devices and sensor applications.

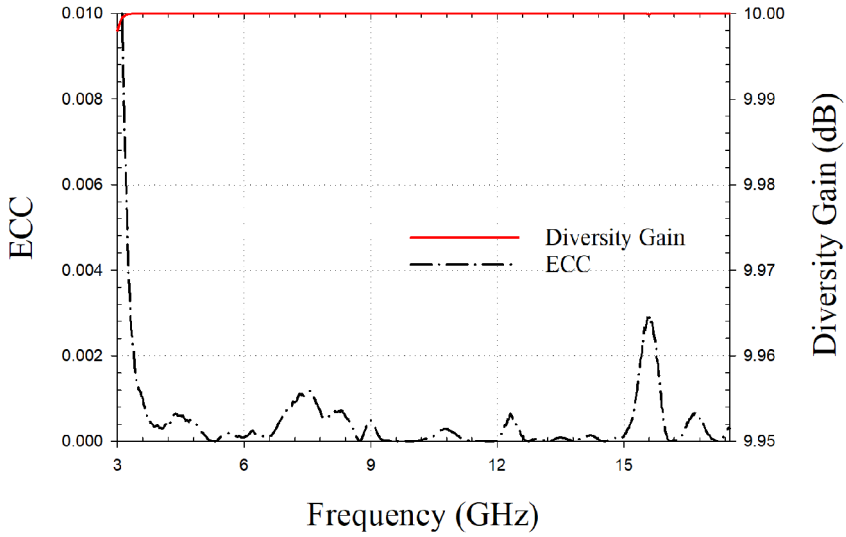

Figure 3-18. Measured ECC and diversity gain of the proposed antenna

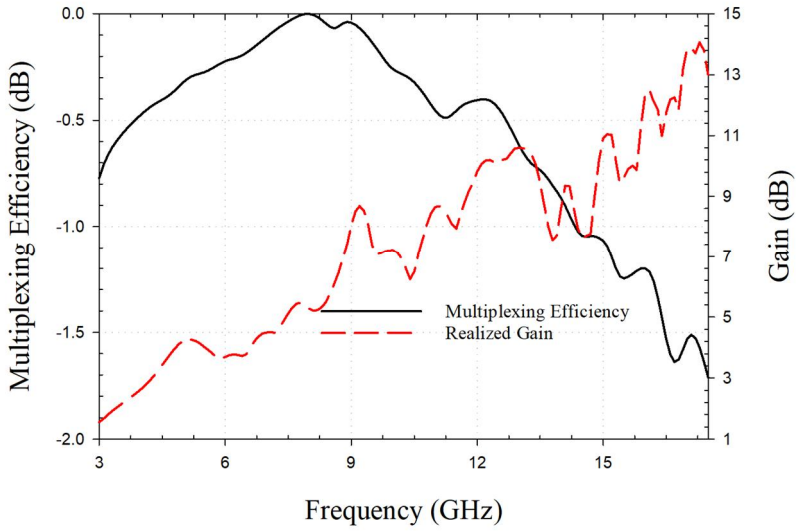

Figure 3-19. Realized gain and radiation efficiency of the antenna

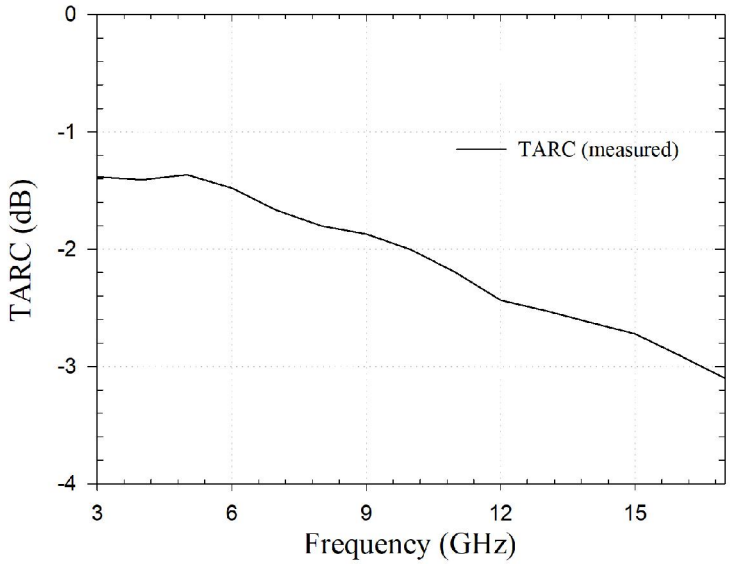

Figure 3-20. TARC for the proposed antenna

b. Comparison with other references

Table 5. Comparison with the recently reported UWB MIMO antenna

Ref.	Size (mm)	Bandwidth (GHz)	Isolation (dB)	ECC	Diversity gain
[34]	30 × 50	2.5□14.5	< −20	< 0.04	> 7.40
[56]	60 × 40	3.1□10.6	< −20	< 0.06	> 9.89
[57]	50 × 80	3.1□10.6	< −17	<0.056	NA
[58]	32 × 32	3.1□10.6	< −15	< 0.04	NA
[59]	26 × 40	2.1□10.6	< −15	NA	NA
[60]	45 × 25	3 □12	<−15	<0.2	> 9.79
Proposed Work	65 × 65	3.1□17.5	< −20	< 0.007	> 9.99

In contrast, the comparison table shows that the proposed antenna demonstrates the better trade-off between bandwidth, Isolation, ECC and diversity gain. Thus, the proposed MIMO antenna can offer simple design and acceptable ultra-wideband MIMO and 5G applications.

4. Conclusion

In this thesis, a microstrip-fed UWB antenna with four-band notch characteristics is presented. First, a UWB antenna was designed to have a 149% bandwidth and operate from 2.9 to 20 GHz by inserting small notches in the ground plane to suppress the upper passband spectrum. Second, four U-shaped slots on the radiating patch were introduced to yield four-band notching to mitigate the electromagnetic interference with WIMAX, the European C-band, INSAT, and WLANs by using the design guidelines that are discussed with corresponding equations. LC equivalent equations are proposed based on analyzing split rings and loop formulas for the regular figure. This methodology allows the antenna designer to choose the selective frequency for rejection and therefore adopt the radiating patch antenna to reject any narrowband system requirement. The measured results from the proposed antenna correspond well with the simulated, theoretical, and LC equivalent analytical notch results. The performance of the antenna is good, with decent impedance matching and VSWR < 2, except at the notch bands. Overall, the presented antenna is suitable for working in a UWB communication system and sensing application, rejecting the narrow bands of frequency.

Similarly, the design of a compact, high-isolation UWB MIMO antenna with a circular parasitic element at the back side of the radiating patch is proposed. Without the presence of a coupling or decoupling element and by introducing a parasitic circular structure, high isolation is achieved at the upper part of the frequency band, whereas a small rectangular notch at the ground plane helps to widen the antenna operating bandwidth and improve the impedance matching of the two connecting radiating elements. To validate the design strategy for reducing mutual coupling and increase the operating bandwidth,

essential features such as ECC (< 0.007), DG (> 9.99), high isolation less than -21 dB, almost omnidirectional radiation pattern and high multiplexing gain performance were shown and verified with simulation and measurement results to describe the MIMO performance of the UWB antenna.

New techniques such as graph model, neural networks can be used to optimize the antenna parameters and design procedure. Smart materials can be used for reconfigurable as it can decrease the size of the antenna and enhance diversity performance. A hybrid antenna such as the frequency with pattern reconfigurable for multiband and added interference rejection can also be designed for better functionality.

Acknowledgment

I would like to express my deepest gratitude to my advisor, Prof. Dong-You Choi, for his support, patience, and encouragement throughout my graduate studied. His technical and editorial advice and words of encouragement and guideless were essential to complete this research successfully.

I am expressing my deep gratitude to my parents, brother and sisters for their love, understanding, supports, and encouragement during the period of this research.

Finally my deepest thanks to my fellow lab mates specially Sujan Shrestha, Iram Nadeem and Janam Maharjan for the simulation discussions, support and their useful suggestion throughout the course of my research.

References

[1] J. Chóliz, Á. Hernández, and A. Valdovinos, "A Framework for UWB-Based Communication and Location Tracking Systems for Wireless Sensor Networks," *Sensors*, vol. 11, no. 9, pp. 9045–9068, 2011.

[2] S. A. Aghdam, "Reconfigurable Antenna With a Diversity Filtering Band Feature Utilizing Active Devices for Communication Systems," *IEEE Transactions on Antennas and Propagation*, vol. 61, no. 10, pp. 5223–5228, 2013.

[3] J. Zhang, P. V. Orlik, Z. Sahinoglu, A. F. Molisch, and P. Kinney, "UWB Systems for Wireless Sensor Networks," *Proceedings of the IEEE*, vol. 97, no. 2, pp. 313–331, 2009.

[4] A. Bekasiewicz and S. Koziel, "Compact UWB monopole antenna for internet of things applications," *Electronics Letters*, vol. 52, no. 7, pp. 492–494, 2016.

[5] B. Allen, M. Dohler, E. Okon, W. Malik, A. Brown, and D. Edwards, "Ultra-Wideband Antennas and Propagation: For Communications, Radar and Imaging," *John Wiley & Sons* , 2006.

[6] K. Y. Yazdandoost and R. Kohno, "UWB antenna for wireless body area network." 2006 Asia-Pacific Microwave Conference. pp. 1647–1652 2006.

[7] G. Adamiuk, T. Zwick, and W. Wiesbeck, "UWB Antennas for Communication Systems," *Proceedings of the IEEE*, vol. 100, no. 7, pp. 2308–2321, 2012.

[8] J. Marimuthu and M. Esa, "Compact UWB PCML bandpass filter with L- and C-shaped resonator," *Electronics Letters*, vol. 44, no. 6, pp. 419–420, 2008.

[9] E. y Jung, J. W. Lee, and C. S. Cho, "Signal Distortion Analysis of L-Shaped UWB Antenna," *IEEE Antennas and Wireless Propagation Letters*, vol. 9, pp. 775–778, 2010.

[10] A. K. Gautam, L. Kumar, B. K. Kanaujia, and K. Rambabu, "Design of Compact F-Shaped Slot Triple-Band Antenna for WLAN/WiMAX Applications," *IEEE Transactions on Antennas and Propagation*, vol. 64, no. 3, pp. 1101–1105, 2016.

[11] J. H. Lu and C. H. Yeh, "Planar Broadband Arc-Shaped Monopole Antenna for UWB System," *IEEE Transactions on Antennas and Propagation*, vol. 60, no. 7, pp. 3091–3095, 2012.

[12] M. Rahman, "CPW fed miniaturized UWB tri-notch antenna with bandwidth enhancement," *Advances in Electrical Engineering*, vol. 2016, 2016.

[13] A. K. Horestani, Z. Shaterian, J. Naqui, F. Martín, and C. Fumeaux, "Reconfigurable and Tunable S-Shaped Split-Ring Resonators and Application in Band-Notched UWB Antennas," *IEEE Transactions on Antennas and Propagation*, vol. 64, no. 9, pp. 3766–3776, 2016.

[14] J. Liu, K. P. Esselle, and S.-S. Zhong, "A printed extremely wideband antenna for multi-band wireless systems." *Antennas and Propagation Society International Symposium (APSURSI)*, 2010 IEEE. pp. 1–4. *IEEE* 2010.

[15] L. Lizzi, F. Viani, R. Azaro, and A. Massa, "Optimization of a Spline-Shaped UWB Antenna by PSO," *IEEE Antennas and Wireless Propagation Letters*, vol. 6, pp. 182–185, 2007.

[16] S. Yadav, A. K. Gautam, and B. K. Kanaujia, "Design of dual band-notched lamp-shaped antenna with UWB characteristics," *International Journal of Microwave and Wireless Technologies*, vol. 9, no. 2, pp. 395–402, 2017.

[17] S. A. Aghdam, "A Novel UWB Monopole Antenna With Tunable Notched Behavior Using Varactor Diode," *IEEE Antennas and Wireless Propagation Letters*, vol. 13, pp. 1243–1246, 2014.

[18] P. Wang, G.-J. Wen, Y.-J. Huang, and Y.-H. Sun, "Compact CPW-fed planar monopole antenna with distinct triple bands for WiFi/WiMAX applications," *Electronics Letters*, vol. 48, no. 7, pp. 357–359, 2012.

[19] M. Sarkar, S. Dwari, and A. Daniel, "Printed Monopole Antenna for Ultra-Wideband Application with Tunable Triple Band-Notched Characteristics," *Wireless Personal Communications*, vol. 84, no. 4, pp. 2943–2954, 2015.

[20] P. Gao, L. Xiong, J. Dai, S. He, and Y. Zheng, "Compact Printed Wide-Slot UWB Antenna With 3.5/5.5-GHz Dual Band-Notched Characteristics," *IEEE Antennas and Wireless Propagation Letters*, vol. 12, pp. 983–986, 2013.

[21] T. Li, H. Zhai, G. Li, L. Li, and C. Liang, "Compact UWB Band-Notched Antenna Design Using Interdigital Capacitance Loading Loop Resonator," *IEEE Antennas and Wireless Propagation Letters*, vol. 11, pp. 724–727, 2012.

[22] W. T. Li, Y. Q. Hei, W. Feng, and X. W. Shi, "Planar Antenna for 3G/Bluetooth/WiMAX and UWB Applications With Dual Band-Notched Characteristics," *IEEE Antennas and Wireless Propagation Letters*, vol. 11, pp. 61–64, 2012.

[23] C. Wang, X. Wei, B. Ding, M. Zhang, D. Wang, Z. He, and Y. Shi, "A band-notched UWB slot antenna with high skirt selectivity and controllable bandwidth." 2014 15th International Conference on Electronic Packaging Technology. pp. 1237–1240, 2014.

[24] Q. X. Chu, C. X. Mao, and H. Zhu, "A Compact Notched Band UWB Slot Antenna With Sharp Selectivity and Controllable Bandwidth," *IEEE Transactions on Antennas and Propagation*, vol. 61, no. 8, pp. 3961–3966, 2013.

[25] Z. h Tu, W. A. Li, and Q. X. Chu, "Single-Layer Differential CPW-Fed Notch-Band Tapered-Slot UWB Antenna," *IEEE Antennas and Wireless Propagation Letters*, vol. 13, pp. 1296–1299, 2014.

[26] A. D. Yaghjian and S. R. Best, "Impedance, bandwidth, and Q of antennas," *IEEE Transactions on Antennas and Propagation*, vol. 53, no. 4, pp. 1298–1324, 2005.

[27] M. A. Jensen and J. W. Wallace, "A review of antennas and propagation for MIMO wireless communications," *IEEE Transactions on Antennas and Propagation*, vol. 52, no. 11, pp. 2810–2824, 2004.

[28] L. Liu, S. W. Cheung, and T. I. Yuk, "Compact MIMO Antenna for Portable Devices in UWB Applications," *IEEE Transactions on Antennas and Propagation*, vol. 61, no. 8, pp. 4257–4264, 2013.

[29] S. K. Dhar, M. S. Sharawi, O. Hammi, and F. M. Ghannouchi, "An Active Integrated Ultra-Wideband MIMO Antenna," *IEEE Transactions on Antennas and Propagation*, vol. 64, no. 4, pp. 1573–1578, 2016.

[30] A. Sharma, G. Das, and R. K. Gangwar, "Design and analysis of tri-band dual-port dielectric resonator based hybrid antenna for WLAN/WiMAX applications," *Antennas Propagation IET Microwaves*, vol. 12, no. 6, pp. 986–992, 2018.

[31] M. T. Hussain, M. S. Sharawi, S. Podilchack, and Y. M. M. Antar, "Closely packed millimeter-wave MIMO antenna arrays with dielectric resonator elements." 2016 10th European Conference on Antennas and Propagation (EuCAP). pp. 1–4, 2016.

[32] M. S. Sharawi, A. B. Numan, M. U. Khan, and D. N. Aloi, "A Dual-Element Dual-Band MIMO Antenna System With Enhanced Isolation for Mobile Terminals," *IEEE Antennas and Wireless Propagation Letters*, vol. 11, pp. 1006–1009, 2012.

[33] R. Karimian, H. Oraizi, S. Fakhte, and M. Farahani, "Novel F-Shaped Quad-Band Printed Slot Antenna for WLAN and WiMAX MIMO Systems," *IEEE Antennas and Wireless Propagation Letters*, vol. 12, pp. 405–408, 2013.

[34] A. Iqbal, O. A. Saraereh, A. W. Ahmad, and S. Bashir, "Mutual Coupling Reduction Using F-Shaped Stubs in UWB-MIMO Antenna," *IEEE Access*, vol. 6, pp. 2755–2759, 2018.

[35] S. F. Jilani and A. Alomainy, "Millimetre-wave T-shaped MIMO antenna with defected ground structures for 5G cellular networks," *Antennas Propagation IET Microwaves*, vol. 12, no. 5, pp. 672–677, 2018.

[36] C. Luo, J. Hong, and L. Zhong, "Isolation Enhancement of a Very Compact UWB-MIMO Slot Antenna With Two Defected Ground Structures," *IEEE Antennas and Wireless Propagation Letters*, vol. 14, pp. 1766–1769, 2015.

[37] Y. Wu and Q. Chu, "Dual-band multiple input multiple output antenna with slitted ground," *Antennas Propagation IET Microwaves*, vol. 8, no. 13, pp. 1007–1013, 2014.

[38] M. A. Abdalla and A. A. Ibrahim, "Compact and Closely Spaced Metamaterial MIMO Antenna With High Isolation for Wireless Applications," *IEEE Antennas and Wireless Propagation Letters*, vol. 12, pp. 1452–1455, 2013.

[39] Q. Li, A. P. Feresidis, M. Mavridou, and P. S. Hall, "Miniaturized Double-Layer EBG Structures for Broadband Mutual Coupling Reduction Between UWB Monopoles," *IEEE Transactions on Antennas and Propagation*, vol. 63, no. 3, pp. 1168–1171, 2015.

[40] Z. Li, Z. Du, M. Takahashi, K. Saito, and K. Ito, "Reducing Mutual Coupling of MIMO Antennas With Parasitic Elements for Mobile

Terminals," *IEEE Transactions on Antennas and Propagation*, vol. 60, no. 2, pp. 473–481, 2012.

[41] S. Zhang and G. F. Pedersen, "Mutual Coupling Reduction for UWB MIMO Antennas With a Wideband Neutralization Line," *IEEE Antennas and Wireless Propagation Letters*, vol. 15, pp. 166–169, 2016.

[42] O. Sydoruk, E. Tatartschuk, E. Shamonina, and L. Solymar, "Analytical formulation for the resonant frequency of split rings," *Journal of Applied Physics*, vol. 105, no. 1, pp. 014903, 2009.

[43] F. E. Terman, "Radio engineers' handbook," 1943.

[44] R. Garg, I. Bahl, and M. Bozzi, "Microstrip lines and slotlines," *Artech house* , 2013.

[45] H. Zhai, L. Liu, Z. Ma, and C. Liang, "A Printed Monopole Antenna for Triple-Band WLAN/WiMAX Applications," *International Journal of Antennas and Propagation*, vol. 2015, p. 7, 2015.

[46] K. A. Alshamaileh, M. J. Almalkawi, and V. K. Devabhaktuni, "Dual Band-Notched Microstrip-Fed Vivaldi Antenna Utilizing Compact EBG Structures," *International Journal of Antennas and Propagation*, vol. 2015, p. 7, 2015.

[47] X. Chen, F. Xu, and X. Tan, "Design of a Compact UWB Antenna with Triple Notched Bands Using Nonuniform Width Slots," *International Journal of Antennas and Propagation*, vol. 2017, p. 9, 2017.

[48] S. Das, D. Mitra, and S. R. B. Chaudhuri, "Design of UWB Planar Monopole Antennas with Etched Spiral Slot on the Patch for Multiple Band-Notched Characteristics," *International Journal of Antennas and Propagation*, vol. 2015, p. 9, 2015.

[49] X. Li, L. Yan, W. Pan, and B. Luo, "A Compact Printed Quadruple Band-Notched UWB Antenna," *International Journal of Antennas and Propagation*, vol. 2013, p. 6, 2013.

[50] D.-O. Kim, N.-I. Jo, H.-A. Jang, and C.-Y. Kim, "Design of the Ultrawideband Antenna with a Quadruple-Band Rejection Characteristics Using a Combination of the Complementary Split Ring Resonators," *Progress In Electromagnetics Research*, vol. 112, pp. 93–107, 2011.

[51] M. Rahman, D.-S. Ko, and J.-D. Park, "A Compact Multiple Notched Ultra-Wide Band Antenna with an Analysis of the CSRR-TO-CSRR Coupling for Portable UWB Applications," *Sensors (Basel, Switzerland)*, vol. 17, no. 10, 2017.

[52] M. S. Sharawi, "Current Misuses and Future Prospects for Printed Multiple-Input, Multiple-Output Antenna Systems [Wireless Corner]," *IEEE Antennas and Propagation Magazine*, vol. 59, no. 2, pp. 162–170, 2017.

[53] S. Blanch, J. Romeu, and I. Corbella, "Exact representation of antenna system diversity performance from input parameter description," *Electronics Letters*, vol. 39, no. 9, pp. 705–707, 2003.

[54] R. Tian, B. K. Lau, and Z. Ying, "Multiplexing efficiency of MIMO antennas in arbitrary propagation scenarios." Antennas and Propagation (EUCAP), 2012 6th European Conference on. pp. 373–377. *IEEE* (2012).

[55] M. Manteghi and Y. Rahmat-Samii, "Multiport characteristics of a wide-band cavity backed annular patch antenna for multipolarization operations," *IEEE Transactions on Antennas and Propagation*, vol. 53, no. 1, pp. 466–474, 2005.

[56] C.-X. Mao, Q.-X. Chu, Y.-T. Wu, and Y.-H. Qian, "Design and Investigation of Closely-Packed Diversity UWB Slot-Antenna with High Isolation," *Progress In Electromagnetics Research*, vol. 41, pp. 13–25, 2013.

[57] S. S. Jehangir and M. S. Sharawi, "A Miniaturized UWB Biplanar Yagi-Like MIMO Antenna System," *IEEE Antennas and Wireless Propagation Letters*, vol. 16, pp. 2320–2323, 2017.

[58] J. Ren, W. Hu, Y. Yin, and R. Fan, "Compact Printed MIMO Antenna for UWB Applications," *IEEE Antennas and Wireless Propagation Letters*, vol. 13, pp. 1517–1520, 2014.

[59] L. Liu, S. W. Cheung, and T. I. Yuk, "Compact MIMO Antenna for Portable Devices in UWB Applications," *IEEE Transactions on Antennas and Propagation*, vol. 61, no. 8, pp. 4257–4264, 2013.

[60] R. Mathur and S. Dwari, "Compact CPW-Fed ultrawideband MIMO antenna using hexagonal ring monopole antenna elements," *AEU - International Journal of Electronics and Communications*, vol. 93, pp. 1–6, 2018.